



How to design potent and selective DYRK1B inhibitors? Molecular modeling study

Agnieszka Szamborska-Gbur¹ · Ewelina Rutkowska¹ · Agnieszka Dreas¹ · Michael Frid² · Maria Vilenchik² · Mariusz Milik¹ · Krzysztof Brzózka¹ · Marcin Król¹

Received: 3 December 2018 / Accepted: 26 December 2018
© Springer-Verlag GmbH Germany, part of Springer Nature 2019

Abstract

DYRK1B protein kinase is an emerging anticancer target due to its overexpression in a variety of cancers and its role in cancer chemoresistance through maintaining cancer cells in the G₀ (quiescent) state. Consequently, there is a growing interest in the development of potent and selective DYRK1B inhibitors for anticancer therapy. One of the major off-targets is another protein kinase, GSK3 β , which phosphorylates an important regulator of cell cycle progression on the same residue as DYRK1B and is involved in multiple signaling pathways. In the current work, we performed a detailed comparative structural analysis of DYRK1B and GSK3 β ATP-binding sites and identified key regions responsible for selectivity. As the crystal structure of DYRK1B has never been reported, we built and optimized a homology model by comparative modeling and metadynamics simulations. Calculation of interaction energies between docked ligands in the ATP-binding sites of both kinases allowed us to pinpoint key residues responsible for potency and selectivity. Specifically, the role of the gatekeeper residues in DYRK1B and GSK3 β is discussed in detail, and two other residues are identified as key to selectivity of DYRK1B inhibition versus GSK3 β . The analysis presented in this work was used to support the design of potent and selective azaindole-quinoline-based DYRK1B inhibitors and can facilitate development of more selective inhibitors for DYRK kinases.

Keywords DYRK1B · GSK3 β · Cancer cell quiescence · Homology modeling · Metadynamics simulations · Kinase inhibitor selectivity

Introduction

Human protein kinases are involved in the vast majority of signal transduction pathways, and aberrations of kinase signaling may lead to the development of many diseases [1]. Consequently, selective inhibition of protein kinases is considered an attractive therapeutic strategy for a wide variety of disorders, including cancer, immunological, neurological, metabolic, and infectious diseases [2, 3]. The number of

publications on development of protein kinase inhibitors is growing steadily and as of this writing the United States Food and Drug Administration (U.S. FDA) approved 43 protein kinase inhibitors,¹ almost all to treat proliferative diseases.

Human protein kinases are divided into conventional and atypical kinases and the former are grouped into eight distinct families based on their sequence similarity in the catalytic domain [4]. Kinases that belong to the CMGC group (named after another set of kinase families – CDK, MAPK, GSK3, and CCLK) are known to be involved in regulation of many therapeutically relevant cellular processes, such as cell cycle progression, cell proliferation, signal transduction, and intracellular communication, among others [5, 6]. CMGC family is composed of several major subfamilies, for which it is named: cyclin-dependent kinases (CDKs), mitogen-activated protein kinases (MAPKs), glycogen synthase kinases (GSKs), CDK-like kinases (CLKs), and dual-specificity tyrosine (Y) phosphorylation-regulated kinases (DYRKs).

Agnieszka Szamborska-Gbur and Ewelina Rutkowska contributed equally to this work.

This paper belongs to Topical Collection 8th conference on Modeling & Design of Molecular Materials (MDMM 2018)

✉ Marcin Król
marcin.krol@selvita.com

¹ Selvita S.A., Bobrzyńskiego 14, 30-348 Kraków, Poland

² FeliciteX Therapeutics, Inc., 27 Strathmore Road, Natick, MA 01760, USA

¹ Data compiled by the Blue Ridge Institute for Medical Research in Horse Shoe, North Carolina USA; <http://www.brimr.org/PKI/PKIs.htm>

The mammalian DYRK subfamily consists of five members divided into two classes. Class I comprises DYRK1A and DYRK1B, while class II is made up of DYRK2, DYRK3, and DYRK4. The most studied member of the subfamily is DYRK1A because of the localization of its gene in the Down-syndrome critical region on chromosome 21 and its association with Down syndrome [7, 8]. Recently, DYRK1A has attracted interest as a target in cancer therapy [9]. DYRK1B is involved in skeletal muscle differentiation [10] and protection against oxidative stress [11]. A growing body of evidence implicates DYRK1B in progression of human cancers [12–17], in which its presence is essential for cancer cell survival [18–22]. DYRK1B regulates the G₀/G₁-S phase transition, and maintains cancer cells in the G₀ phase of the cell cycle, a quiescent state also called cellular dormancy [17, 23–27]. There is ample evidence that diminution of DYRK1B activity, on either functional or expression levels, can induce cell cycle re-entry of quiescent cancer cells, thus making these cells vulnerable to standard chemotherapeutics [18, 28, 29]. DYRK1B exerts negative regulatory effects on cell cycle re-entry via its substrates, cyclin D1 and p27^{Kip1} — phosphorylation by DYRK1B destabilizes cyclin D1 and stabilizes p27^{Kip1}. Some of these effects on the molecular level are also exerted by DYRK1A through its facilitation of the dimerization partner, RB-like, E2F, and multi-vulval class B (DREAM) complex assembly, and the relative contribution of either A or B isoform to cell cycle regulation appears to depend on the specific tissue and experimental system [17]. Consequently, selective inhibitors of DYRK1A/B are the focus of drug development projects in cancer therapy via the quiescence axis and as tool compounds to investigate the role of DYRK1A/B in cancer cell dormancy. It is noteworthy that recent research findings indicate that DYRK2 plays a role in GSK3 β -dependent degradation of c-Jun and c-Myc transcription factors by ‘priming phosphorylation’ [30]. Thus, several DYRK kinases are involved in cell cycle control and quiescence.

Access to selective compounds is crucial in all stages of drug discovery effort. While it is not mandatory for a successful therapeutic to have a clean selectivity profile, as exemplified by several approved kinase inhibitors, it clearly helps to elucidate the target’s role in the disease model [31]. Additionally, in the lead optimization stage off-target activity may lead to undesired toxic effects [32], which need to be removed before progressing to the clinic. In the case of kinase inhibitors, obtaining selectivity is not a trivial task, as virtually all active compounds target the ATP-binding site, which is highly conserved among human protein kinases. One way to deal with the issue is to profile compounds of interest against a representative or a comprehensive set of off-targets in vitro [33, 34], and various studies indicate that the development of selective compounds targeting the ATP pocket is possible [35, 36]. An alternative or a complementary tactic is to apply

one or several computational strategies developed specifically to design selective kinase inhibitors. These methods range from QSAR-type approaches that are aimed at predicting response on a large number of kinases [37, 38] to structure-based methods that are usually limited in the number of kinases studied but take into consideration information on structural differences between on- and off-targets [39, 40], including subtle solvation effects [41]. Design of selective kinase inhibitors is also facilitated by several databases containing detailed data on kinase-ligand interactions in the ATP-binding site [42].

When designing selective DYRK1 inhibitors, natural off-targets are other members of the CMGC family, such as CDKs, CLKs, and GSK3s. Glycogen synthase kinase-3 (GSK3) refers to two paralogs, GSK3 α and GSK3 β . The latter is a constitutively active kinase with over 100 known protein substrates, by far the most substrates to be phosphorylated by a single kinase. As a consequence, GSK3 β is involved in many different regulatory pathways and has become an attractive target in developing treatments for multiple types of diseases. Additionally, there are multiple regulatory mechanisms involved in controlling its substrate-specific actions, which further add to the complex biology of this target [43]. GSK3 β is a particularly important off-target kinase in any project that aims at development of potent DYRK1 inhibitors acting via the quiescence axis as it phosphorylates cyclin D1 at Thr286 similarly to DYRK1B [44] and is known to be active in quiescent cells.

In this work we describe the identification of structural features of DYRK1B kinase that allows designing potent and selective DYRK1B inhibitors, with particular focus on selectivity over GSK3 β kinase. As no structural details have been published for DYRK1B, we employed comparative modeling procedure. Here, we report a DYRK1B homology model and compare it structurally with a crystal structure of GSK3 β . Such comparative analysis may aid in the identification of structural differences between both proteins that can be used for rendering selectivity. Subsequently, we use a set of internally developed DYRK1B inhibitors with specific substitution patterns that probe the subspaces of the ATP-binding pocket identified by the comparative analysis. Docking studies enable the identification of the key residues responsible for the selectivity and validate their importance in terms of binding energy analysis. Finally, we propose structural guidelines that facilitate design of selective DYRK1B inhibitors.

Materials and methods

DYRK1B homology model generation

Homology modeling of human DYRK1B was performed using the knowledge-based method in Prime, Schrödinger

software [45]. The amino acid sequence of the target was obtained from UniProt database (Q9Y463) [46]. Protein backbone and side chains were directly copied to the model from the template's conserved residues. Optimization of side chains and minimization of nontemplate residues were performed using a standard procedure for homology modeling in Prime. No ligand structures were used for either homology modeling or final refinement of the DYRK1A-based homology model. Finally, a short minimization of the protein structure was performed with convergence of heavy atoms set to 0.30 Å RMSD and full flexibility of hydrogen atoms.

Analysis of available crystal structures of DYRK1A indicated two possible conformations of Phe170 (Phe122 in DYRK1B), an apical residue of the glycine-rich loop, termed Phe-IN and Phe-OUT (Fig. 1). This residue plays a key role in the opening of the loop. Consequently, ten homology models for each conformation of Phe122 were built and the lowest-energy models for Phe-IN and Phe-OUT were taken for further development. A detailed description of template selection is given in "Results and discussion".

Binding pose metadynamics

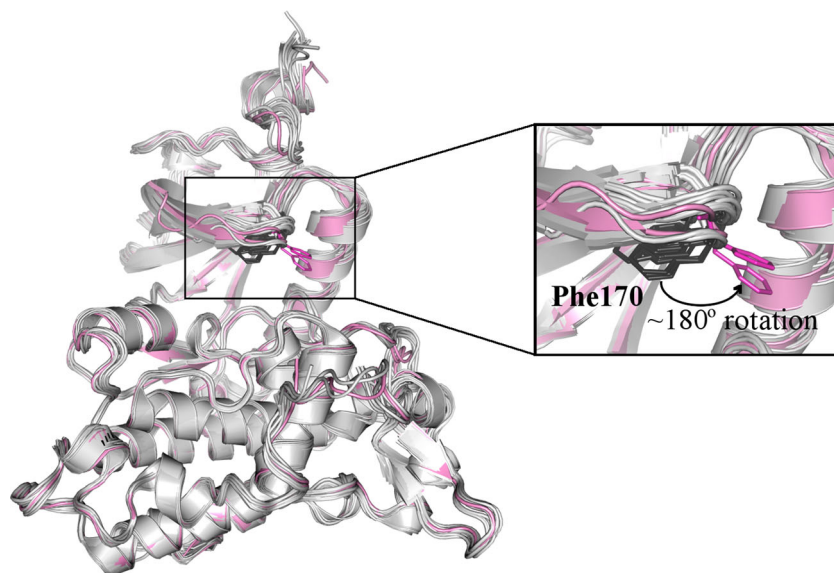
To verify the correct conformation of Phe122 residue in DYRK1B a set of binding configurations of a single ligand in two homology models (Phe-IN and Phe-OUT conformation in each protein model) was subjected to metadynamics simulations. Metadynamics is a widely used enhanced sampling method that allows sampling of complex free energy landscapes [47]. The metadynamics protocol applied in this work uses a time-dependent bias as a function of the chosen collective variable to enhance sampling of the ligand movements in and around its binding pose. This type of simulation assisted

us in providing insight into proper glycine-rich loop conformation depending on the bound ligand. Ten trials of 10 ns metadynamics simulations per each protein-ligand complex were performed according to the binding pose metadynamics protocol from the Schrödinger package [48]. No constraints were used in the simulations. Each trial reported here was run using the Desmond program from the Schrödinger package on a single GPU card, taking 6 h per trial for a given system.

Docking

Docking grids were generated using the receptor grid generation module in Glide application [49]. Grids were generated with OPLS3 force field [50], keeping the default values of van der Waals scaling factor set to 0.8 and charge cutoff set to 0.15. The binding site was defined based on GSK3 β -bound ligand. A cubic box of 10 Å dimension centered around the inhibitor in the active site was generated for each protein structure. The LigPrep and Epik modules from the Schrödinger suite [51] were used to prepare ligands for docking. Their ionization states were generated at pH 7.0 \pm 2.0. Three low energy conformers per ligand were generated and docked to the protein using Glide docking protocol with extra precision (XP) mode. Docking strategy included writing per-residue interaction energy values in order to determine key residues involved in ligand binding and selectivity. Ligands were docked to DYRK1B and GSK3 β models and the docking poses with the best Glide scores were analyzed. Compounds which showed favorable interactions and good Glide score along with acceptable expected physicochemical properties were then selected for synthesis.

Fig. 1 Side chain rearrangement of Phe170 residue in DYRK1A upon binding of ligands with different sizes. Phe170 residue is presented in sticks, while Phe-IN and Phe-OUT conformations are shown in dark gray and pink, respectively. PDB codes for the two DYRK1A crystal structures with Phe-OUT conformations are 2WO6 and 4MQ1 [52, 53]



Results and discussion

DYRK1B homology model

Two homology models of DYRK1B kinase domain were built based upon the homologous DYRK1A protein having 85% sequence identity within the kinase domain. When human DYRK1A structures were 3D aligned, the most striking difference within the kinase active site was observed at the glycine-rich loop in the Phe170 conformation (Phe122 residue in DYRK1B; see Figs. 1 and 3d). Phe170 rotates approximately 180 degrees away to make space for a chlorophenyl group in both 4MQ1 and 2WO6 structures [52, 53] (Phe-OUT conformation), while it is in a buried position (Phe-IN conformation) in the remaining 16 human DYRK1A crystal structures (Fig. 1). Thus, the Phe170 residue can adapt its conformation upon ligand binding since it does not encounter any significant steric hindrance.

Analysis of available DYRK1A inhibitors indicates that conformation of Phe170 can be affected by ligand binding. To address two major conformational states of this residue we selected two DYRK1A crystal structures as templates for homology modeling with the following PDB codes: 5A4T (Phe-IN) and 4MQ1 (Phe-OUT) [52, 54]. Selection of the templates was carried out based on the analysis of DYRK1A-ligand interactions in the Protein-Ligand Database [55]. Generation and refinement of the DYRK1B homology models relied on their high sequence identity to the DYRK1A templates. Amino acid composition of ATP-binding pockets in these isoforms is almost identical. The only amino acid substitution, Leu240 in DYRK1A into Met192 in DYRK1B, influenced neither hinge conformation nor ligand interactions. Although Phe122 conformation was inspected for each model in our homology modeling study, it is assumed that known DYRK1A inhibitors will bind similarly in the DYRK1B ATP-binding pocket [56, 57].

Pose stability assessment — DYRK1B homology model validation

In a homology modeling procedure the essential step is a careful selection of a template protein. To date, there are 18 human DYRK1A structures deposited in the PDB [58]. As mentioned above, the most striking difference that can be observed among DYRK1A structures is the side chain rearrangement of Phe170 belonging to the glycine-rich loop. To examine the most probable orientation of the Phe170 residue and to assess stability of DYRK1B model structures (Phe-IN and Phe-OUT) in complex with an inhibitor, a series of metadynamics simulations were employed. In the first place, we selected one of the ligands from our initial series (structure not shown) and docked into the two homology models according to the procedure described in “Materials and methods”.

Next, following the metadynamics protocol, ten independent short simulations were performed, through which the average RMSD deviation from the starting pose was calculated [48]. The results are summarized in Fig. 2.

The results were assessed both for pose stability based on the ligand RMSD with respect to the anchor fragment and the initial internal ligand coordinates and for the persistence of hydrogen bonds between the ligand and the protein. PoseScore is a score that measures how close the pose stays to its initial pose in terms of RMSD. This metric showed higher stability for the complex of DYRK1B with Phe122 in the ‘IN’ conformation. The persistence of the starting contact network can provide a useful complementary metric that can predict instability of poses in cases where the RMSD estimate has not fully captured information about the instability. A

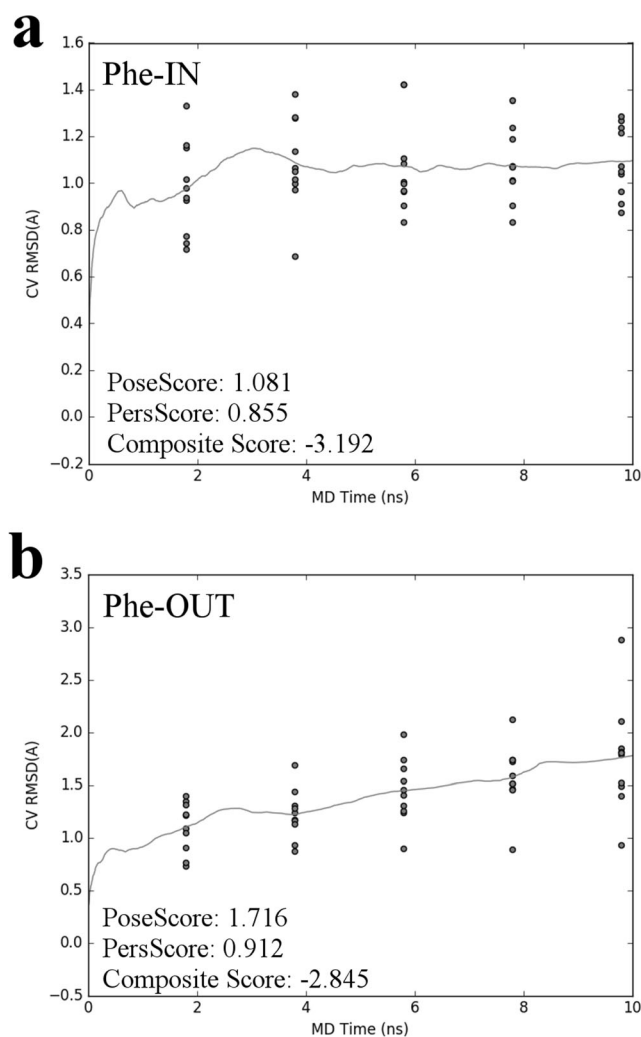


Fig. 2 Binding pose metadynamics metrics for an exemplary ligand bound to two DYRK1B homology models. **a)** DYRK1B model with Phe122-IN conformation. **b)** DYRK1B model with Phe122-OUT conformation. The dots represent RMSD values at various points in time for each of the 10 simulations. The line represents the average value at each point in time. Significance of the scores is described in the text

complementary parameter, PersScore, measures the persistence of interactions (hydrogen bonds and π -cation) in terms of the normalized number of interactions with respect to the starting pose over the course of the simulation. PersScore value calculated for DYRK1B with Phe-IN conformation was lower than for the Phe-OUT DYRK1B model. However, before normalization over four hydrogen bonds (H-bonds), the Phe-IN DYRK1B model results in a total PersScore value of 3.42. The DYRK1B Phe-OUT model was normalized per three H-bonds, giving a total PersScore value equal to 2.74, indicating its lower stability. Moreover, in the latter complex the interaction with the Ser194 residue was missing due to a slight difference in side chain arrangement in the binding pocket. Composite score (CompScore) is an additional metric that tends to balance the PoseScore and PersScore contributions. This parameter was calculated as follows:

$$\text{CompScore} = \text{PoseScore} - 5 \cdot \text{PersScore}$$

Lower values of all the PoseScore, PersScore, and CompScore parameters obtained for the first protein-ligand complex structure (Phe-IN) showed this structure to be more stable and consequently more probable to occur for the investigated series of DYRK1B inhibitors.

In conclusion, the analysis of the metadynamics results showed that the complex of an inhibitor and a homology model built on the DYRK1A template (PDB code: 5A4T) [54] with 'IN' conformation of Phe122 was more structurally stable and would better represent the inhibition profiles described by our experimental data. Therefore, we relied on this model for subsequent stages of our study.

GSK3 β crystal structure selection

In the following step we performed the analysis of GSK3 β crystal structures in order to select the most suitable protein structure for our docking study. We analyzed all GSK3 β crystal structures collected in the PDB [58] that include ligands structurally similar to our DYRK1B inhibitors. Resolution below 3.0 Å, data released in the last 10 years, and a small number of missing residues were the primary parameters used for the selection of representative structures. In addition, we focused on flexibility of the glycine-rich loop, looking especially at conformation of the Phe67 residue located at the beta hairpin turn of the glycine-rich loop equivalent to Phe122 in DYRK1B. As a result, four GSK3 β crystal structures with a high diversity of glycine-rich loop conformations were selected for further analysis. In the next step, a set of our DYRK1B inhibitors that revealed a strong inhibitory effect on GSK3 β were docked into the four protein structures (data not shown). Finally, one GSK3 β crystal structure (PDB code: 4PTE) [59] with Phe67 in the Phe-IN conformation, which provided us

with the most reliable docking results, was chosen based on interactions with the hinge region and Lys85 residue.

Binding site comparison between DYRK1B and GSK3 β structures

Selectivity over GSK3 β was one of the key objectives in the development of potent DYRK1B kinase inhibitors reported in this paper. In order to distinguish major structural features responsible for the selectivity, a comparative analysis of the ATP-binding site of DYRK1B and its off-target GSK3 β was performed (Fig. 3). Both DYRK1B and GSK3 β structures adopt the typical kinase bi-lobed fold, which is characterized by the N-terminal domain consisting mainly of β -strands and a single α -helix, whereas the C-terminal domain is primarily α -helical (Fig. 3a). The two lobes are connected by a flexible hinge region and separated by a deep cleft comprising the ATP-binding site. Although many amino acid residues forming the pocket are highly conserved among protein kinase families [60], some of them differ between DYRK1B and GSK3 β . Below we describe three regions of the ATP-binding pocket that differ between these enzymes and can be used to design selective inhibitors.

The amino acid sequence of the hinge is F¹⁹⁰ELLSYN in DYRK1B and L¹³²DYVPET in GSK3 β . As is apparent from the sequences, the gatekeeper is a bulky phenylalanine in DYRK1B and a branched hydrophobic leucine in GSK3 β . These residues differ in shape and chemical character (aromatic vs aliphatic) and, therefore, the gatekeeper region can be targeted for obtaining selectivity. However, it should be noted that the bulky gatekeeper residue in DYRK1B limits exploration of the back pocket to small substituents only, thus rendering the search for selectivity in this region difficult (see Fig. 3a–c).

The buried region of the ATP pocket [61] is formed by a similar set of hydrophobic residues in both kinases, mostly occupied by leucines and valines (Fig. 3c). There is one notable substitution in this region — Val258 (DYRK1B) into Cys199 (GSK3 β), which is suggested as a leading cause of kinase inhibitor selectivity [62–65]. The Cys199 residue that directly precedes the DFG motif is also targeted in the development of GSK3 β irreversible inhibitors [66–68].

A high proportion of conserved residues is reported within the phosphate region of the ATP-binding pocket. Next to the DFG motif, Glu155, Lys140, and Asn244 are conserved in both kinases (numbering according to DYRK1B). Importantly, phenylalanine is an aromatic residue at the beta hairpin turn of the glycine-rich loop that affects the ligand binding in both DYRK1B and GSK3 β (Phe122 and Phe67, respectively). The entrance to the ATP pocket is built by a set of polar amino acid residues. The solvent exposed region is formed by the lower portion of the hinge and the glycine-rich loop together with a spacious area of polar residues on the C-

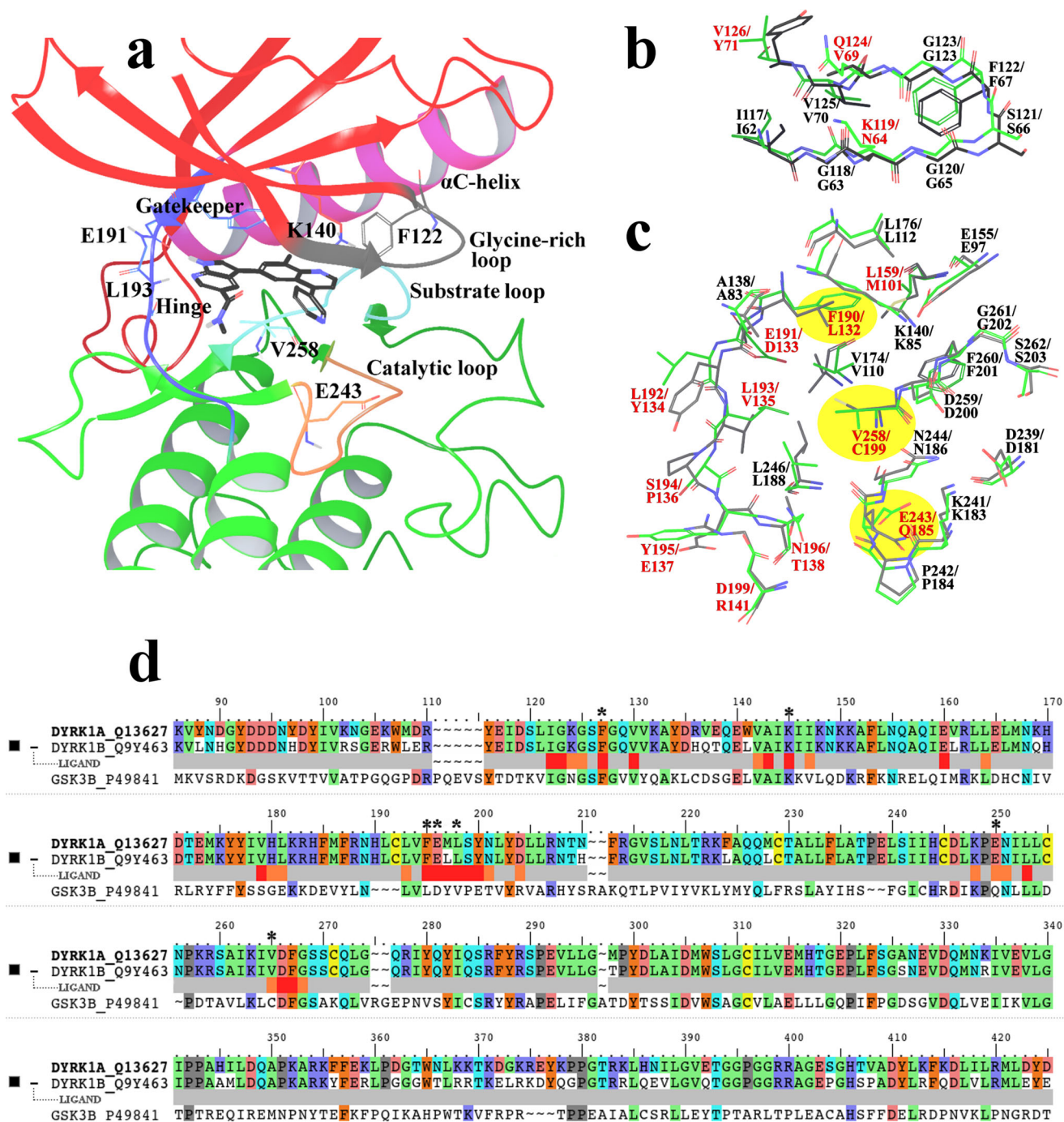


Fig. 3 Comparison between DYRK1B homology model and GSK3 β crystal structure (PDB code: 4PTE). **a**) General view of the DYRK1B kinase domain structure complexed with compound 4B (black sticks). Two lobes, a helix-rich C-terminal lobe and a sheet-rich N-terminal lobe are presented in green and red, respectively. The ATP-binding pocket is located at the interface of the two lobes. Hinge is shown in blue, glycine-rich loop in gray, catalytic loop in orange, substrate loop in cyan, and α C-helix in pink. The amino acid residues involved in the inhibitor binding are presented in sticks. **b**) Structural alignment of glycine-rich loop residues. DYRK1B is shown in green and GSK3 β in

black. Residues that differ from DYRK1B and GSK3 β are labeled in red. **c**) Structural alignment of the ATP-binding pocket without the glycine-rich loop (presented separately in b). Key sequence differences discussed in the present work are marked in yellow. **d**) Sequence alignment for DYRK1B, DYRK1A (as a template for homology modeling), and GSK3 β kinases. LIGAND row shows the DYRK1B residues involved in binding of compound 4B: red and orange rectangles for residues interacting with the ligand up to 4 and 6 Å, respectively. Black asterisks indicate the F122, K140, F190, E191, L193, E243, and V258 residues shown in sticks in panel a)

lobe part of the binding site. Differences in side chains' polarity may cause a wide range of possible interactions with

ligands. Special attention should be given to two positions in the hinge region: i) the phenol group of Tyr195 in DYRK1B

in comparison with the carboxylic group of Glu137 in GSK3 β , ii) the amide group of Asn196 in DYRK1B versus the hydroxyethyl group of Thr138 in GSK3 β . There is also a negatively charged Asp199 side chain, which differentiates DYRK1B from GSK3 β , in which a positively charged guanidinium group of Arg141 occupies the same position. The Glu137 and Arg141 residues in GSK3 β form a salt bridge that effectively decreases the size of the binding site opening to the solvent. The opposite part of the ATP pocket's entrance is also formed by alternately negatively and positively charged residues involved in strong long-range Coulomb interactions: Asp239, Lys241, and Glu243 in DYRK1B and similarly Asp181, Lys183, and Gln185 in GSK3 β . The electrostatic difference between the Glu243 and Gln185 residues can also be a suitable anchorage point for the selective DYRK1B inhibitor design.

Development of selective DYRK1B inhibitors

A subset of project compounds with very good activity against DYRK1B in the low nanomolar range and varying activity against GSK3 β was docked to the selected DYRK1B homology model and GSK3 β crystal structure. Encouragingly, all docked ligands showed very good scores and favorable interactions within the ATP-binding pocket of DYRK1B, in agreement with our experimental data [69]. Here, we present a detailed analysis of the binding mode and ligand-protein interactions in the active sites of both enzymes with the aim of explaining observed differences in GSK3 β activity.

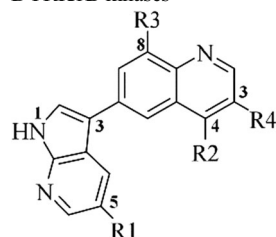
The analysis of top-ranking compounds according to the docking score allowed us to classify designed inhibitors into two groups with respect to R3 modification on the quinoline moiety at position 8 and one group with respect to R2 modification on the quinoline moiety at position 4 (Table 1). The

first group with fluorine substituent in the R3 position was termed series A, the second group bearing methyl group – series B, and the third group having positively charged R2 substituents – series C. Analysis of the data collected in Table 1 shows that compounds belonging to series A are not selective against GSK3 β , while replacement of fluorine by methyl group (series B) or attachment of a positively charged functional group in position R2 (series C) leads to highly selective compounds. In order to explain the observed experimental results, we examined binding interactions of R2 and R3 substituents in all compound series in both enzymes.

Analysis of protein-ligand interactions observed for series A, B, and C consistently show two strong hydrogen bonds with the hinge residues (Glu191, Leu193, numbering according to DYRK1B) formed in both enzymes. In DYRK1B, the Phe190 phenyl group stabilizes the position of ligands' core via π - π interactions with the quinoline moiety (Fig. 4), while replacement of Phe by Leu residue removes this interaction in GSK3 β . The quinoline N atom forms H-bond with the Lys140 -amine group. Interaction with this residue, present in both enzymes (Lys140 in DYRK1B and Lys85 in GSK3 β), is often formed by different kinase inhibitors, as Lys residue in this sequence position is highly conserved across the kinome. In addition to the aforementioned interactions, the compounds also form van der Waals interactions with aliphatic residues Val125, Leu193, Val174, Leu246, and Val258 (numbering according to DYRK1B sequence) (see Fig. 3). The attractive forces between the azaindole-quinoline core and Val258 side chain require careful attention [65] and are discussed below.

The key difference between the enzymes in the region interacting with R3 substituent is the gatekeeper residue — Phe190 in DYRK1B and Leu132 in GSK3 β . The planar aromatic side chain of Phe190 allows methyl group of series B to fit between the phenyl plane and Lys140 (compare Figs. 4a

Table 1 Comparison of three groups of azaindole-quinoline derivatives (series A, B, and C of potent DYRK1B inhibitors) and their activity toward GSK3 β and DYRK1B kinases



Compound	R1	R2	R3	R4	GSK3 β %INH (1 μ M)	DYRK1B %INH (1 μ M)
1A	H	H	F	H	65	99
1B	H	H	CH ₃	H	7	>90
2A	H	Ph	F	H	93	99
2B	H	Ph	CH ₃	H	26	92
3A	H	3-Py	F	H	94	100
3B	H	3-Py	CH ₃	H	27	95
4A	CO-NH-CH ₃	3-Py	F	H	97	99
4B	CO-NH-CH ₃	3-Py	CH ₃	H	36	90
1C	H	NH-Pip-CH ₃	H	H	1	>90
2C	H	NH-Pip-CH ₃	H	CN	8	>90
3C	H	N(CH ₃)-Pip-CH ₃	H	NO ₂	6	>90
4C	H	NH-(<i>c</i>)Cy-(<i>e</i>)-NH ₂	H	H	5	90

Ph – phenyl, Py – pyridine, Pip – piperidine, Cy – cyclohexyl, %INH (1 μ M) – percentage of inhibition at 1 μ M of an inhibitor

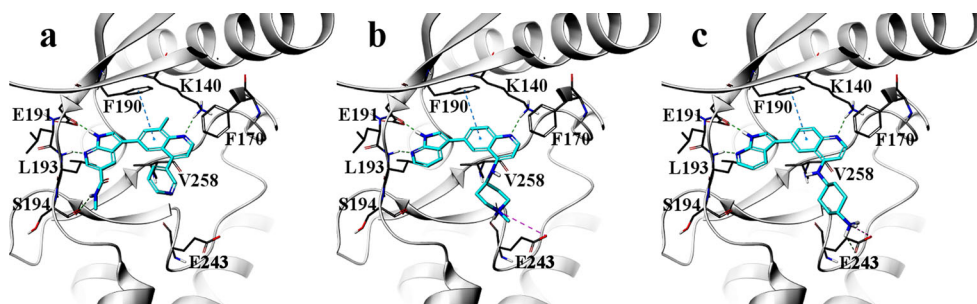


Fig. 4 Docking poses of selected DYRK1B inhibitors in DYRK1B homology model structure. **a)** Compound 4B, **b)** compound 1C, **c)** compound 4C. The key residues involved in interactions with the

ligands are labeled. Hydrogen bonds are presented as green dashed lines, salt bridges as pink dashed lines, and π - π stacking interactions with the gatekeeper residue as blue dashed lines

and 5a). On the contrary, replacement of the flat phenyl ring of Phe190 by a branched isobutyl side chain of Leu132 in GSK3 β pointing into the ATP pocket results in steric repulsion between the ligand's methyl group in position R3 and the isobutyl group of Leu132 (Fig. 5b). As a consequence, series B ligands can bind deeper in the DYRK1B pocket compared with GSK3 β (Fig. 5c), which has several important implications for the strength of the protein-ligand interactions. First, deeper binding of series B ligands in DYRK1B allows for decreasing the distance between quinoline N atom and Lys140, thus increasing the strength of the hydrogen bond. Additionally, there is a stronger interaction between the R3 methyl group and aromatic ring of Phe190 compared to aliphatic isobutyl of Leu132. To quantify this effect, we calculated van der Waals interaction energy between gatekeeper residues in both enzymes and selected compounds from series A and B (Table 2). The van der Waals (vdW) energy term reflects hydrophobic interactions between a ligand and an amino acid residue. Strikingly, our potent DYRK1B inhibitors exhibiting low GSK3 β activity (see compounds 1B–4B presented in Table 1 and Table 2) consistently displayed favorable vdW interaction energy values with Phe190 in DYRK1B, while interaction energies with Leu132 in GSK3 β vary from weakly stabilizing (compounds 1B and 3B) to destabilizing

(compounds 2B and 4B). Consequently, we conclude that the volume of the methyl group in position R3 and its interactions with gatekeeper residues of both enzymes are the primary drivers for the selectivity observed in series B.

It was also interesting to investigate the lack of selectivity observed for series A. First, the fluorine atom in position R3 is smaller compared to the methyl group [70], and the steric repulsive effect in GSK3 β is therefore diminished. This is confirmed by the comparison of binding poses of series A compounds in both enzymes, which are virtually identical (data not shown). Additionally, the fluorine atom interacts more strongly with the ϵ -amine group of Lys140 residue present in both kinases compared to the methyl group due to fluorine's high electronegativity. Therefore, we claim that not only the steric bulk of the R3 substituent but also the strength of its inductive effect is crucial for strong and specific interactions with DYRK1B and GSK3 β kinases.

Replacement of a fluorine substituent by a methyl group, which forms only weak London dispersion interactions, has an impact on diverse biological responses, including selectivity among bioreceptors, increased potency, and metabolic stability [71]. Methyl groups are expected to increase the lipophilicity of a ligand molecule. Their introduction or removal may significantly alter the pharmacological activity of the

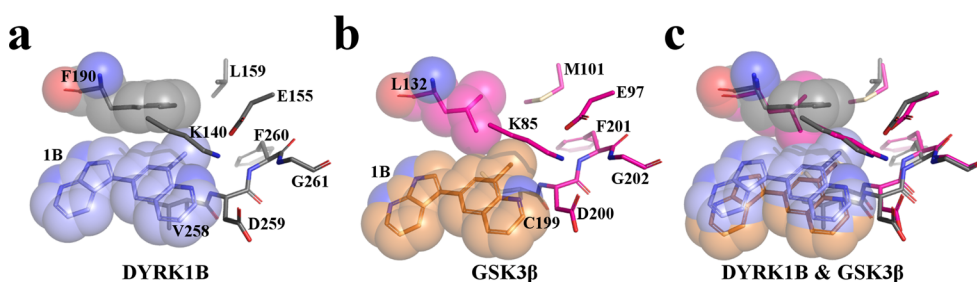


Fig. 5 Binding mode of the DYRK1B inhibitor bearing methyl group in quinoline moiety at position 8 (compound 1B) in DYRK1B (gray) and GSK3 β (pink) structures. The ligand structure and the gatekeeper residue are shown as vdW spheres. **a)** Docking pose obtained for DYRK1B homology model. The conformation of a planar aromatic side chain of Phe190 enables the inhibitor (blue) to be located deeply in the ATP pocket. Side chain of Val258 residue is located directly underneath the quinoline part of the molecule and forms hydrophobic interactions with the

ligand's core. **b)** Docking result obtained for GSK3 β crystal structure (PDB code 4PTE). Branched aliphatic side chain of Leu132 keeps the ligand molecule (orange) farther from the back pocket residues. Side chain of Cys199 residue interacts with the methyl group of the ligand. **c)** Superimposition of both protein-ligand complex structures presented in panels a) and b). The shift between the docked compound 1B in the ATP pocket is visible. For clarity no residue labels were added

Table 2 Van der Waals energy terms for interactions between selective DYRK1B inhibitors (series B) and two selected residues: gatekeeper and the residue that directly precedes the DFG motif (position DFG-1).Coulomb energy term for interaction of series C and the selected residue located in the solvent exposed region. Energy values are presented in kcal mol⁻¹

Compound	Gatekeeper		DFG-1 position		Compound	Solvent exposed region	
	Phe190 DYRK1B	Leu132 GSK3 β	Val258 DYRK1B	Cys199 GSK3 β		Glu243 DYRK1B	Gln185 GSK3 β
1B	-3.9	-2.0	-3.8	-3.3	1C	-31.5	-0.4
2B	-3.7	1.6	-4.2	-3.3	2C	-33.6	-0.1
3B	-4.0	-1.8	-4.2	-2.2	3C	-31.8	-1.5
4B	-3.9	0.6	-4.2	-3.4	4C	-47.4	-0.7

compound, leading to different pharmacokinetic and pharmacodynamic profiles [72]. Moreover, there are numerous literature examples of methyl group substitutions that were successfully introduced to achieve selectivity between two therapeutic target subtypes [73, 74]. Introduction of a methyl group into the R3 position of our compounds led to the development of the highly selective series B of DYRK1B inhibitors.

The azaindole part of our ligands contacts the hinge region via two hydrogen bonds with the backbones of Glu191 and Leu193 or Asp133 and Val135 residues in DYRK1B and GSK3 β , respectively. Side chains of these residues are directed to the outside of the binding pocket. Furthermore, the replacement of Ser194 (DYRK1B) with Pro136 (GSK3 β) residue in the gatekeeper +4 position of hinge changes the overall conformation of the hinge and makes the GSK3 β hinge more rigid than that of DYRK1B due to the restricted nature of one of the dihedral angles of proline caused by the cyclization of its side chain. The carbonyl group of Ser194 backbone exposed to the ATP pocket may provide an additional interaction point for inhibitors bearing the *N*-methylcarbamoyl group in the R1 position (see compounds 4A and 4B in Table 1). Such an additional H-bond between the R1 substituent and the hinge (in particular Ser194 backbone) is shown in Fig. 4a. In the studied set of compounds, two other hinge residues, namely Tyr195 and Asn196 in DYRK1B compared to Glu137 and Thr138 in GSK3 β , affect the binding of the ligands to a lesser extent due to limited modifications in the R1 position.

Another structural difference that can be targeted to achieve selectivity for DYRK1B over GSK3 β is the Val258 residue in DYRK1B compared to Cys199 in the corresponding position in GSK3 β structure. Val258 is probably one of the most significant hot spot residues that differentiates DYRK1B from its off-targets. According to the Kinase Sequence Database, this DFG-1 position is occupied by a valine residue only in 2% of the entire kinome, in comparison with 9.5% for cysteine and 32% for alanine residue [75]. As mentioned above, our inhibitors can bind deeply in the DYRK1B ATP pocket. As a consequence, the Val258 residue is located directly underneath the quinoline moiety and forms hydrophobic interactions with the ligand's core (Fig. 5a). In contrast, the inhibitors bind

shallower in the GSK3 β ATP pocket. The side chain of the Cys199 residue interacts mainly with the R3 substituent (Fig. 5b). Differences in mutual orientation of the ligands' core and the DFG-1 residue (Val258 in DYRK1B and Cys199 in GSK3 β) contribute to different selectivity profiles observed for the inhibitors toward the two kinases (see compound 1B in Fig. 5c and Table 1).

To quantify the effect of structural change in this position we calculated the vdW interaction energy term between the selective ligands and Val258 in DYRK1B and Cys199 in GSK3 β (Table 2). Analysis of data collected in the third column of Table 2 indicates that our selective DYRK1B inhibitors (series B) consistently display more favorable vdW energy values for Val258 in DYRK1B compared to Cys199 in GSK3 β . This effect adds to the more favorable interaction energy of series B in the gatekeeper region and further increases selectivity of this group of compounds.

Sampling of R2 substituents within our azaindole-quinoline core showed that neither phenyl nor 3-pyridyl moieties improve the inhibitors' specificity toward GSK3 β (see compounds 2A and 3A in Table 1). One of the groups that causes a drop in the off-target activity is 4-amino-1-methylpiperidine introduced at position 4 of quinoline moiety. Compound 1C presented in Fig. 4b displays only 1% of inhibition on GSK3 β at 1 μ M, while retaining its low nanomolar activity against DYRK1B. Analysis of binding interactions for this compound indicates that a positively charged nitrogen atom in the piperidine ring interacts with the Glu243 residue in DYRK1B and forms a salt bridge. This salt bridge cannot be formed in GSK3 β due to Glu243 to Gln185 substitution. Consequently, this mutation is yet another sequence variation between the analyzed enzymes that contributes to the selectivity over GSK3 β in our series of inhibitors. This effect is further confirmed by compound 2C bearing the same 4-amino-1-methylpiperidine in position R2 and displaying 8% of inhibition on GSK3 β at 1 μ M (see Table 1). Similar effects involving a salt bridge with Glu243 were observed for compounds 3C and 4C (Fig. 4c) with *N*-methyl(1-methylpiperidin-4-yl)amino and (4-aminocyclohexyl)amino positively charged groups in position R2, displaying 6% and

5% of inhibition on GSK3 β at 1 μ M, respectively (Table 1). This observation was supported by Coulomb interaction energy values collected from our docking study (see compounds 1C–4C in Table 1 and Table 2). For series C inhibitors interaction energy values were more favorable for binding to DYRK1B. It should be noted that all C series compounds retained low nanomolar activity on DYRK1B.

In summary, focusing our design efforts on regions of the ATP-binding site that structurally differ between DYRK1B and GSK3 β we developed a potent and highly selective group of compounds (series B and C). Three amino acid residues within the DYRK1B ATP pocket are crucial for the high affinity and selectivity of series B and C compounds; these are Phe190, Val258, and Glu243. It should be noted that none of our selective compounds interacts with all three residues, with series B targeting Phe190 and Val258, and series C targeting Glu243. Consequently, analysis of activity and selectivity profiles of compounds that interact with all three residues described above would be of utmost importance and will be reported in the future.

Conclusions

The design of selective inhibitors remains an important and difficult field in scientific and pharmaceutical research. Developing selective inhibitors for protein kinases is in general a challenge; the close similarity among kinase domains and the conserved structure of ATP-binding sites across kinome makes it difficult to design selective compounds. In principle, highly selective inhibitors can be developed by targeting substrate binding sites or allosteric binding sites, the amino acid sequences and structures of which vary considerably. However, these sites are not always available, may be difficult to locate, or may not be druggable. Consequently, targeting the ATP-binding site is the most direct approach to identify kinase inhibitors. In the present work, we employed structural comparative analysis to study key structural features of ATP pockets in the project-related kinases by molecular modeling simulations. We identified several regions in the ATP pocket responsible for selective binding of designed inhibitors. Through examination of per-residue interaction energy values we pinpointed key residues responsible for the ligand binding and for the enzyme selectivity. In the case of DYRK1B and GSK3 β , the key DYRK1B residues for selectivity are the gatekeeper Phe190, Val258 that directly precedes the DFG motif, and Glu243 located in the solvent exposed region. The first two residues influence the hydrophobic interactions with our inhibitors, while Glu243 forms a salt bridge with the positively charged substituents in the R2 position of the ligands. To conclude, a detailed analysis of structural models supported by evaluation of interaction energy values helped to elucidate the putative binding mode and infer the

basis of selectivity for the investigated series of azaindole-quinoline-based compounds. This work further confirms that structural analysis supplemented with molecular modeling may serve as a powerful tool to design potent and selective kinase inhibitors.

Acknowledgements This work was supported by the European Union from the European Regional Development Fund within the frame Operational Programme Innovative Economy (Grant No. UDA-POIG.01.04.00-12-048/11-00). Project title: *New pharmacotherapy of neurodegenerative diseases: innovative kinase inhibitors*.

Compliance with ethical standards

Conflict of interest The authors declare that they have no conflict of interest.

Publisher's Note Springer Nature remains neutral with regard to jurisdictional claims in published maps and institutional affiliations.

References

- Cohen P (2002) Protein kinases—the major drug targets of the twenty-first century? *Nat Rev Drug Discov* 1:309–315
- Zhang J, Yang PL, Gray NS (2009) Targeting cancer with small molecule kinase inhibitors. *Nat Rev Cancer* 9:28–39. <https://doi.org/10.1038/nrc2559>
- Fedorov O, Muller S, Knapp S (2010) The (un)targeted cancer kinome. *Nat Chem Biol* 6:166–169
- Manning G, Whyte DB, Martinez R, Hunter T, Sudarsanam S (2002) The protein kinase complement of the human genome. *Science* 298:1912–1934. <https://doi.org/10.1126/science.1075762>
- Varjosalo M, Keskitalo S, Van Drogen A, Nurkkala H, Vichalkovski A, Aebersold R, Gstaiger M (2013) The protein interaction landscape of the human CMGC kinase group. *Cell Rep* 3: 1306–1320
- Singh R, Lauth M (2017) Emerging roles of DYRK kinases in embryogenesis and hedgehog pathway control. *J Dev Biol* 5:13–28. <https://doi.org/10.3390/jdb5040013>
- Park J, Song W-J, Chung KC (2009) Function and regulation of Dyrk1A: towards understanding down syndrome. *Cell Mol Life Sci* 66:3235–3240. <https://doi.org/10.1007/s00018-009-0123-2>
- Rosse G (2013) Tricyclic pyrimidines as inhibitors of DYRK1A/DYRK1B as potential treatment for Down's syndrome or Alzheimer's disease. *ACS Med Chem Lett* 4:502–503
- Ionescu A, Dufresne F, Gelbcke M, Jabin I, Kiss R, Lamoral-Theys D (2012) DYRK1A kinase inhibitors with emphasis on cancer. *Mini Rev Med Chem* 12:1315–1329. <https://doi.org/10.2174/13895575112091315>
- Mercer S, Friedman E (2006) Mirk/Dyrk1B: a multifunctional dual-specificity kinase involved in growth arrest, differentiation, and cell survival. *Cell Biochem Biophys* 45:303–315
- Deng X, Mercer SE, Sun C-Y, Friedman E (2014) The normal function of the cancer kinase Mirk/dyrk1B is to reduce reactive oxygen species. *Genes Cancer* 5:22–30. <https://doi.org/10.18632/genesandcancer.1>
- Chen Y, Wang S, He Z, Sun F, Huang Y, Ni Q, Wang H, Wang Y, Cheng C (2017) Dyrk1B overexpression is associated with breast cancer growth and a poor prognosis. *Hum Pathol* 66:48–58. <https://doi.org/10.1016/j.humpath.2017.02.033>

13. Friedman E (2010) The kinase Mirk/dyrk1B: a possible therapeutic target in pancreatic cancer. *Cancers (Basel)* 2:1492–1512. <https://doi.org/10.3390/cancers2031492>
14. Gruber W, Hutzinger M, Elmer DP, Parigger T, Sternberg C, Cegielski L, Zaja M, Leban J, Michel S, Hamm S, Vitt D, Aberger F (2016) DYRK1B as therapeutic target in hedgehog/GLI-dependent cancer cells with smoothed inhibitor resistance. *Oncotarget* 7:7134–7148. <https://doi.org/10.18632/oncotarget.6910>
15. Mercer SE, Ewton DZ, Shah S, Naqvi A, Friedman E (2006) Mirk/Dyrk1b mediates cell survival in rhabdomyosarcomas. *Cancer Res* 66:5143–5150. <https://doi.org/10.1158/0008-5472.CAN-05-1539>
16. Singh R, Dhanyamraju PK, Lauth M (2017) DYRK1B blocks canonical and promotes non-canonical hedgehog signaling through activation of the mTOR/AKT pathway. *Oncotarget* 8:833–845. <https://doi.org/10.18632/oncotarget.13662>
17. Becker W (2018) A wake-up call to quiescent cancer cells – potential use of DYRK1B inhibitors in cancer therapy. *FEBS J* 285:1203–1211. <https://doi.org/10.1111/febs.14347>
18. Li L, Liu Y, Zhang Q, Zhou H, Zhang Y, Yan B (2014) Comparison of cancer cell survival triggered by microtubule damage after turning Dyrk1B kinase on and off. *ACS Chem Biol* 9:731–742. <https://doi.org/10.1021/cb4005589>
19. Friedman E (2007) Mirk/Dyrk1B in cancer. *J. Cell. Biochem.* 102:274–279. <https://doi.org/10.1002/jcb.21451>
20. Mercer SE, Friedman E (2006) Mirk/Dyrk1B: a multifunctional dual-specificity kinase involved in growth arrest, differentiation, and cell survival. *Cell Biochem Biophys* 45:303–315. <https://doi.org/10.1385/CBB:45:3:303>
21. Gao J, Zheng Z, Rawal B, Schell MJ, Bepler G, Haura EB (2009) Mirk/Dyrk1B, a novel therapeutic target, mediates cell survival in non-small cell lung cancer cells. *Cancer Biol Ther* 8:1671–1679. <https://doi.org/10.4161/cbt.8.17.9322>
22. Gao J, Yang X, Yin P, Hu W, Liao H, Miao Z, Pan C, Li N (2012) The involvement of FoxO in cell survival and chemosensitivity mediated by Mirk/Dyrk1B in ovarian cancer. *Int J Oncol* 40:1203–1209. <https://doi.org/10.3892/ijo.2011.1293>
23. Friedman E (2013) The kinase MIRK/DYRK1B mediates a reversible quiescent state in a subset of ovarian, pancreatic and colon cancers. In: Hayat M (ed) *Tumor dormancy, quiescence, and senescence*. Springer, Dordrech, pp 117–126
24. Hu J, Nakhla H, Friedman E (2011) Transient arrest in a quiescent state allows ovarian cancer cells to survive suboptimal growth conditions and is mediated by both Mirk/dyrk1b and p130/RB2. *Int J Cancer* 129:307–318. <https://doi.org/10.1002/ijc.25692>
25. Zou Y, Ewton DZ, Deng X, Mercer SE, Friedman E (2004) Mirk/dyrk1B kinase destabilizes cyclin D1 by phosphorylation at threonine 288. *J Biol Chem* 279:27790–27798. <https://doi.org/10.1074/jbc.M403042200>
26. Gao J, Zhao Y, Lv Y, Chen Y, Wei B, Tian J, Yang Z, Kong F, Pang J, Liu J, Shi H (2013) Mirk/Dyrk1B mediates G0/G1 to S phase cell cycle progression and cell survival involving MAPK/ERK signaling in human cancer cells. *Cancer Cell Int* 13:2–9. <https://doi.org/10.1186/1475-2867-13-2>
27. Ewton DZ, Hu J, Vilenchik M, Deng X, Luk K-c, Polonskaia A, Hoffman AF, Zipf K, Boylan JF, Friedman EA (2011) Inactivation of Mirk/Dyrk1b kinase targets quiescent pancreatic cancer cells. *Mol Cancer Ther* 10:2104–2114. <https://doi.org/10.1158/1535-7163.MCT-11-0498>
28. Kettle JG, Ballard P, Bardelle C, Cockerill M, Colclough N, Critchlow SE, Debreczeni J, Fairley G, Fillery S, Graham MA, Goodwin L, Guichard S, Hudson K, Ward RA, Whittaker D (2015) Discovery and optimization of a novel series of dyrk1b kinase inhibitors to explore a MEK resistance hypothesis. *J Med Chem* 58:2834–2844. <https://doi.org/10.1021/acs.jmedchem.5b00098>
29. Hu J, Deng H, Friedman EA (2013) Ovarian cancer cells, not normal cells, are damaged by Mirk/Dyrk1B kinase inhibition. *Int J Cancer* 132:2258–2269. <https://doi.org/10.1002/ijc.27917>
30. Taira N, Mimoto R, Kurata M, Yamaguchi T, Kitagawa M, Miki Y, Yoshida K (2012) DYRK2 priming phosphorylation of c-Jun and c-Myc modulates cell cycle progression in human cancer cells. *J Clin Invest* 122:859–872. <https://doi.org/10.1172/JCI60818DS1>
31. Frye SV (2010) The art of the chemical probe. *Nat Chem Biol* 6:159–161. <https://doi.org/10.1038/nchembio.296>
32. Lounkine E, Keiser MJ, Whitebread S, Mikhailov D, Hamon J, Jenkins JL, Lavan P, Weber E, Doak AK, Côté S, Shoichet BK, Urban L (2012) Large-scale prediction and testing of drug activity on side-effect targets. *Nature* 486:361–367. <https://doi.org/10.1038/nature11159>
33. Bain J, Plater L, Elliott M, Shpiro N, Hastie CJ, McLauchlan H, Kleveric I, Arthur JSC, Alessi DR, Cohen P (2007) The selectivity of protein kinase inhibitors: a further update. *Biochem J* 408:297–315. <https://doi.org/10.1042/BJ20070797>
34. Bamborough P, Drewry D, Harper G, Smith GK, Schneider K (2008) Assessment of chemical coverage of kinome space and its implications for kinase drug discovery. *J Med Chem* 51:7898–7914. <https://doi.org/10.1021/jm8011036>
35. Anastassiadis T, Deacon SW, Devarajan K, Ma H, Peterson JR (2011) Resource comprehensive assay of kinase catalytic activity reveals features of kinase inhibitor selectivity. *Nat Biotechnol* 29:1039–1045. <https://doi.org/10.1038/nbt.2017>
36. Davis MI, Hunt JP, Herrgard S, Ciceri P, Wodicka LM, Pallares G, Hocker M, Treiber DK, Zarrinkar PP (2011) Comprehensive analysis of kinase inhibitor selectivity. *Nat Biotechnol* 29:1046–1051. <https://doi.org/10.1038/nbt.1990>
37. Sheridan RP, Nam K, Maiorov VN, McMasters DR, Cornell WD (2009) QSAR models for predicting the similarity in binding profiles for pairs of protein kinases and the variation of models between experimental data sets. *J Chem Inf Model* 49:1974–1985
38. Martin E, Mukherjee P, Sullivan D, Jansen J (2011) Profile-QSAR: a novel meta-QSAR method that combines activities across the kinase family to accurately predict affinity, selectivity, and cellular activity. *J Chem Inf Model* 51:1942–1956
39. Ravichandran S, Luke BT, Collins JR (2015) Can structural features of kinase receptors provide clues on selectivity and inhibition? A molecular modeling study. *J Mol Graph Model* 57:36–48. <https://doi.org/10.1016/j.jmgm.2014.12.007>
40. Davare MA, Vellere NA, Wagner JP, Eide CA, Goodman JR (2015) Structural insight into selectivity and resistance profiles of ROS1 tyrosine kinase inhibitors. *Proc Natl Acad Sci U S A* 112:5381–5390. <https://doi.org/10.1073/pnas.1515281112>
41. Levinson NM, Boxer SG (2014) A conserved water-mediated hydrogen bond network defines bosutinib's kinase selectivity. *Nat Chem Biol* 10:127–132. <https://doi.org/10.1038/nchembio.1404>
42. van Linden OPJ, Kooistra AJ, Leurs R, de Esch IJP, de Graaf C (2014) KLIFS: a knowledge-based structural database to navigate kinase-ligand interaction space. *J Med Chem* 57:249–277. <https://doi.org/10.1021/jm400378w>
43. Beurel E, Grieco SF, Jope RS (2015) Pharmacology & Therapeutics Glycogen synthase kinase-3 (GSK3): regulation, actions, and diseases. *Pharmacol Ther* 148:114–131. <https://doi.org/10.1016/j.pharmthera.2014.11.016>
44. Ashford A, Oxley D, Kettle JG, Hudson K, Guichard S, Cook S, Lochhead P (2014) A novel DYRK1B inhibitor AZ191 demonstrates that DYRK1B acts independently of GSK3 β to phosphorylate cyclin D1 at Thr286, not Thr288. *Biochem J* 457:43–56
45. Schrödinger, LLC (2018) Schrödinger release 2018-1: Prime. Schrödinger, LLC, New York
46. Boutet E, Lieberherr D, Tognolli M, Schneider M, Bairoch A (2007) UniProtKB/Swiss-Prot. *Methods Mol Biol* 406:89–112

47. Laio A, Parrinello M (2002) Escaping free-energy minima. *Proc Natl Acad Sci* 99:12562–12566
48. Clark AJ, Tiwary P, Borrelli K, Feng S, Miller EB, Abel R, Friesner RA, Berne BJ (2016) Prediction of protein–ligand binding poses via a combination of induced fit docking and Metadynamics simulations. *J Chem Theory Comput* 12:2990–2998. <https://doi.org/10.1021/acs.jctc.6b00201>
49. Schrödinger, LLC (2018) Schrödinger release 2018-1: Glide. Schrödinger, LLC, New York
50. Harder E, Damm W, Maple J, Wu C, Reboul M, Xiang JY, Wang L, Lupyan D, Dahlgren MK, Knight JL, Kaus JW, Cerutti DS, Krilov G, Jorgensen WL, Abel R, Friesner RA (2016) OPLS3: a force field providing broad coverage of drug-like small molecules and proteins. *J Chem Theory Comput* 12:281–296. <https://doi.org/10.1021/acs.jctc.5b00864>
51. Schrödinger, LLC (2018) Schrödinger release 2018-1: LigPrep, Epik. Schrödinger, LLC, New York
52. Anderson K, Chen Y, Chen Z, Dominique R, Glenn K, He Y, Janson C, Luk KC, Lukacs C, Polonskaia A, Qiao Q, Raikar A, Rossman P, Sun H, Xiang Q, Vilenchik M, Wovkulich P, Zhang X (2013) Pyrido[2,3-d]pyrimidines: discovery and preliminary SAR of a novel series of DYRK1B and DYRK1A inhibitors. *Bioorganic Med Chem Lett* 23:6610–6615. <https://doi.org/10.1016/j.bmcl.2013.10.055>
53. Soundararajan M, Roos AK, Savitsky P, Filippakopoulos P, Kettenbach AN, Olsen JV, Gerber SA, Eswaran J, Knapp S, Elkins JM (2013) Structures of down syndrome kinases, DYRKs, reveal mechanisms of kinase activation and substrate recognition. *Structure* 21:986–996. <https://doi.org/10.1016/j.str.2013.03.012>
54. Rothweiler U, Stensen W, Brandsdal BO, Isaksson J, Leeson FA, Eng H, Svendsen JSM (2016) Probing the ATP-binding pocket of protein kinase DYRK1A with Benzothiazole fragment molecules. *J Med Chem* 59:9814–9824. <https://doi.org/10.1021/acs.jmedchem.6b01086>
55. Schrödinger, LLC (2018) Schrödinger release 2018-1: Protein-Ligand Database (PLDB). Schrödinger, LLC, New York
56. Ruben K, Wurzlbauer A, Walte A, Sippl W, Bracher F, Becker W (2015) Selectivity profiling and biological activity of novel β -carbolines as potent and selective DYRK1 kinase inhibitors. *PLoS One* 10:1–18. <https://doi.org/10.1371/journal.pone.0132453>
57. Meine R, Becker W, Falke H, Preu L, Loaċ N, Meijer L, Kunick C (2018) Indole-3-carbonitriles as DYRK1A inhibitors by fragment-based drug design. *Molecules* 23:1–23. <https://doi.org/10.3390/molecules23020064>
58. Berman HM, Westbrook J, Feng Z, Gilliland G, Bhat TN, Weissig H, Shindyalov IN, Bourne PE (2000) The protein data bank. *Nucleic Acids Res* 28:235–242. <https://doi.org/10.1093/nar/28.1.235>
59. Sivaprakasam P, Han X, Civiello RL, Jacutin-Porte S, Kish K, Pokross M, Lewis HA, Ahmed N, Szapiel N, Newitt JA, Baldwin ET, Xiao H, Krause CM, Park H, Nophsker M, Lippy JS, Burton CR, Langley DR, Macor JE, Dubowchik GM (2015) Discovery of new acylaminopyridines as GSK-3 inhibitors by a structure guided in-depth exploration of chemical space around a pyrrolopyridinone core. *Bioorganic Med Chem Lett* 25:1856–1863. <https://doi.org/10.1016/j.bmcl.2015.03.046>
60. Norman RA, Toader D, Ferguson AD (2012) Structural approaches to obtain kinase selectivity. *Trends Pharmacol Sci* 33:273–278. <https://doi.org/10.1016/j.tips.2012.03.005>
61. Vulpetti A, Bosotti R (2004) Sequence and structural analysis of kinase ATP pocket residues. *Farmacologia* 59:759–765. <https://doi.org/10.1016/j.farmac.2004.05.010>
62. Maqbool M, Mobashir M, Hoda N (2016) Pivotal role of glycogen synthase kinase-3: a therapeutic target for Alzheimer's disease. *Eur J Med Chem* 107:63–81
63. Schmitt C, Kail D, Mariano M, Empting M, Weber N, Paul T, Hartmann RW, Engel M (2014) Design and synthesis of a library of lead-like 2,4-bisheterocyclic substituted thiophenes as selective Dyrk/Clk inhibitors. *PLoS One* 9:e87851. <https://doi.org/10.1371/journal.pone.0087851>
64. Vulpetti A, Crivori P, Cameron A, Bertrand J, Brasca MG, D'Alessio R, Pevarello P (2005) Structure-based approaches to improve selectivity: CDK2-GSK3 β binding site analysis. *J Chem Inf Model* 45:1282–1290. <https://doi.org/10.1021/ci0500280>
65. Fischer PM (2003) CDK versus GSK-3 inhibition. A purple haze no longer? *Chem Biol* 10:1144–1146. <https://doi.org/10.1016/j.chembiol.2003.12.009>
66. Dominguez JM, Fuertes A, Orozco L, Del M-MM, Delgado E, Medina M (2012) Evidence for irreversible inhibition of glycogen synthase kinase-3 β by tideglusib. *J Biol Chem* 287:893–904. <https://doi.org/10.1074/jbc.M111.306472>
67. Kramer T, Schmidt B, Lo Monte F (2012) Small-molecule inhibitors of GSK-3: structural insights and their application to Alzheimer's disease models. *Int J Alzheimers Dis* 2012:381029
68. Li X, Wang X, Tian Z, Zhao H, Liang D, Li W, Qiu Y, Lu S (2014) Structural basis of valmerins as dual inhibitors of GSK3 β /CDK5. *J Mol Model* 20:1–11. <https://doi.org/10.1007/s00894-014-2407-1>
69. Dreas A, Fabritius CH, Dzienia A, Buda A, Gałczowski M, Kachkovskiy G, Kulesza U, Kucwaj-Brysz K, Szamborska-Gbur A, Czardybon W, Vilenchik M, Frid M, Kuznetsova A (2018) Quinoline-1H-pyrrolo[2, 3-b] pyridine derivatives as inhibitors of DYRK1A and/or DYRK1B kinases and their preparation, pharmaceutical compositions and use in the treatment of diseases. Patent No. WO 2018119039 (A1)
70. Böhm H-J, Banner D, Bendels S, Kansy M, Kuhn B, Müller K, Obst-Sander U, Stahl M (2004) Fluorine in medicinal chemistry. *Chembiochem* 5:637–643. <https://doi.org/10.1002/cbic.200301023>
71. Barreiro EJ, Kümmerle AE, Fraga CAM (2011) The methylation effect in medicinal chemistry. *Chem Rev* 111:5215–5246. <https://doi.org/10.1021/cr200060g>
72. Bazzini P, Wermuth CG (2008) In the practice of medicinal chemistry. Academic, San Diego, pp 431–463
73. Kim S-K, Fristrup P, Abrol R, Goddard WA (2011) Structure-based prediction of subtype selectivity of histamine H3 receptor selective antagonists in clinical trials. *J Chem Inf Model* 51:3262–3274. <https://doi.org/10.1021/ci200435b>
74. Aleksandra M, Robert V (2017) What a difference a methyl group makes: the selectivity of monoamine oxidase B towards histamine and N-methylhistamine. *Chem – A Eur J* 23:2915–2925. <https://doi.org/10.1002/chem.201605430>
75. Buzko O, Shokat KM (2002) A kinase sequence database: sequence alignments and family assignment. *Bioinformatics* 18:1274–1275